Journal of Magnetic Resonance **150,** 137–146 (2001)
doi:10.1006/jmre.2001.2322, available online at http://www.idealibrary.com on IDEAL®

Separating Structure and Dynamics in CSA/DD Cross-Correlated Relaxation: *A Case Study on Trehalose and Ubiquitin*

Katalin E. Kövér*,[1] and Gyula Batta†

*Department of Chemistry, University of Debrecen, P.O. Box 21, H-4010 Debrecen, Hungary; and †Research Group for Antibiotics of the Hungarian Academy of Sciences, P.O. Box 70, H-4010 Debrecen, Hungary

Received September 26, 2000; revised March 9, 2001; published online May 15, 2001

We present two new sensitivity enhanced gradient NMR experiments for measuring interference effects between chemical shift anisotropy (CSA) and dipolar coupling interactions in a scalar coupled two-spin system in both the laboratory and rotating frames. We apply these methods for quantitative measurement of longitudinal and transverse cross-correlation rates involving interference of ^{13}C CSA and ^{13}C–^{1}H dipolar coupling in a disaccharide, α,α-D-trehalose, at natural abundance of ^{13}C as well as interference of amide ^{15}N CSA and ^{15}N–^{1}H dipolar coupling in uniformly ^{15}N-labeled ubiquitin. We demonstrate that the standard heteronuclear T_1, T_2, and steady-state NOE autocorrelation experiments augmented by cross-correlation measurements provide sufficient experimental data to quantitatively separate the structural and dynamic contributions to these relaxation rates when the simplifying assumptions of isotropic overall tumbling and an axially symmetric chemical shift tensor are valid.

Key Words: **chemical shift anisotropy; dynamics; NMR relaxation; relaxation interference.**

INTRODUCTION

Due to the recent developments of isotope labeling strategies coupled with the introduction of gradient enhanced multidimensional NMR experiments, there is a renewed interest in the study of heteronuclear relaxation and relaxation interference between different relaxation mechanisms in macromolecules (*1–13*). The typically measured heteronuclear relaxation parameters, T_1, T_2, and NOE, have primarily been analyzed using the "model-free" approach of Lipari and Szabo (*14, 15*) in which the relaxation rates are fitted with a minimal number of dynamic parameters, including the generalized order parameter, S^2, a correlation time for internal motion, τ_e, and an overall correlation time, τ_c. Extensions of this model considering the anisotropy of the global rotational diffusion tensor and the possibility of two-time-scale internal motion have also been proposed (*16, 17*). However, the assumption of a uniform ^{15}N chemical shift anisotropy (CSA) value in the description of the chemical anisotropy relaxation contribution is becoming more apparent as a limitation of this formalism, as several recent investigations demonstrate that both the orientation and the principal values of chemical shift tensor can significantly vary from residues to residues in a protein (*18–21*). Our approach presented here requires no *a priori* assumptions on the value of CSA, considering instead the magnitude and orientation of the chemical shift tensor as variables. We demonstrate that an extension of the model-free Lipari–Szabo formalism which is based on the simultaneous analysis of five heteronuclear relaxation data, T_1, T_2, NOE, η_{zz}, and η_{xy}, where η_{zz} and η_{xy} denote the longitudinal and transverse cross-correlation rates, respectively, allows the evaluation of both the dynamics and the chemical shift anisotropy parameters, including separation of the magnitude and orientation terms of CSA.

Recently, several applications of longitudinal and/or transverse relaxation interference between chemical shift anisotropy and dipolar interactions have been described. It was demonstrated that the ratios of the transverse and longitudinal cross-correlation rates allow a more accurate description of molecular motions, irrespective of any structural parameters such as internuclear distances or chemical shift tensors (*11*). Moreover, the combined use of longitudinal and transverse CSA/DD relaxation interference has been proposed for unambiguous separation of chemical exchange contributions to transverse relaxation from that of rotational diffusion anisotropy (*22*). It has also been shown that the angular dependence of the η_{xy} and η_{zz} ratio of macromolecules of known three-dimensional structure provides a more reliable measure of rotational anisotropy than that of the corresponding R_2/R_1 ratio (*23–25*) because the interference terms are free of exchange contributions. All of these studies and several others (not mentioned here) underline the importance of cross-correlation effects as a sensitive indicator of molecular dynamics. However, it is also well known that the strength of the relaxation interference between CSA and DD interactions depends on the principal values and orientation of the chemical shift tensor as well (*26*). Structural information arising from evaluation of cross-correlated relaxation rates in terms of CSA projections was found to be invaluable for the description of subtle variations in local conformation or characterization

[1] To whom correspondence should be addressed. Fax: +36-52-489-667. E-mail: kover@tigris.klte.hu.

1090-7807/01 $35.00

of H-bond strength (*5, 7, 8*). It is well established now that the chemical shift tensor is more sensitive to conformational changes than the averaged isotropic chemical shift. However, the evaluation of CSA from cross-correlated relaxation rates requires *a priori* knowledge of the dynamics. To this end, the global and local dynamic parameters are derived from the standard T_1, T_2, and heteronuclear NOE data using the Lipari–Szabo formalism and assuming an average value of −160 ppm CSA for the amide ^{15}N. In the case of ^{13}C relaxation studies, the CSA relaxation contributions are generally omitted except for aromatic/olefinic carbons. With the dynamic behavior known, the CSA projections (or geometry-dependent CSA, CSA_g (*27*)) can be determined from the cross-correlation rates based on the well-known equations (*26, 28*) (see below). The major limitation of this approach, that a uniform CSA must be assumed for evaluation of dynamics and then the derived dynamic parameters are used for evaluation of individual CSAs, was recently resolved by Fushman and Cowburn and colleagues (*18, 19*). They propose a dynamic-free approach for the evaluation of CSA parameters which is based on measuring transverse auto- and cross-correlation relaxation rates at different static magnetic fields. This method, however, suffers from the inherent disadvantage of multiple-field experiments: it is very sensitive to errors due to mismatching of experimental conditions on different spectrometers (*42*). Using published experimental data we found that 1–2% error in one of the four relaxation parameters results in a significant variation (ca. 5–10%) in the CSA terms. According to our experience, accuracy better than 3–5% in the cross-correlated relaxation rates can hardly be achieved even when the greatest care is taken in the selection of experimental parameters.

In order to circumvent the above limitations of the multiple-field approach, we propose an extension of the Lipari–Szabo formalism which is simply based on simultaneous evaluation of five relaxation measurements performed at one magnetic field strength in terms of dynamic and CSA parameters. We apply this approach to the analysis of ^{13}C relaxation rates measured in α,α-D-trehalose at natural abundance of ^{13}C and to the evaluation of ^{15}N relaxation rates measured in uniformly ^{15}N-labeled ubiquitin. In addition, we propose new sensitivity enhanced gradient methods for the measurement of longitudinal and transverse cross-correlation rates, which are generally applicable to molecules of any size and do not require specific isotopic enrichment.

RESULTS AND DISCUSSION

Pulse Sequences for Quantitative Measurement of Longitudinal and Transverse CSA/DD Cross-Correlation Rates

The experimental techniques available for measuring longitudinal and transverse cross-correlation rates of dipolar X–H and X–CSA relaxation interference generally require isotopic enrichment and are mostly applicable to macromolecules (*8, 10, 11, 22, 29, 30*). In order to minimize possible complications resulting from multispin effects, high-level deuteration of protons which do not actively participate in the interactions of interest is also recommended. Typically, two or even more separate measurements are required for recording the reference spectra which are devoid of relaxation interference effects.

The pulse schemes we propose here show excellent performance on both isotopically enriched and natural abundance samples and are applicable to molecules of any size. The adverse effect of spin diffusion is avoided by measuring the initial buildup rate of the interference effect (*31, 32*). The largely similar pulse sequences proposed for the measurement of η_{zz} and η_{xy} permit the design of one common reference experiment. The experiments have been tested on small to medium-sized molecules in the fast to intermediate motional regime and large biomolecules with slow tumbling. The pulse schemes for measuring η_{zz} and η_{xy} are depicted in Figs. 1A and 1B together with the reference experiment (Fig. 1C) used for the measurement of the initial magnetization state. The experiments are simply based on an INEPT/reverse INEPT gradient sensitivity enhancement pulse scheme (*33*) and basically correspond to the two-dimensional extensions of our earlier 1D experiments (*27, 34, 35*) with the inclusion of gradients for the suppression of undesired coherences and selection of the desired ones. First, an initial INEPT period transfers equilibrium I_z magnetization into $2I_zS_z$ two-spin order, which is converted further to $2I_zS_y$ antiphase coherence only in the transverse cross-correlation relaxation measurement. The gradient pulses, G_1 and G_2, serve to generate a pure initial magnetization state prior to the τ delay by destroying any undesired coherences. During the relaxation time period τ, relaxation interference between dipolar and CSA interactions mediates the conversion of $2I_zS_z$ coherence to S_z (Fig. 1A) or $2I_zS_y$ to S_y (Fig. 1B), respectively. In the transverse (rotating frame, ortho-ROESY (*36*)) cross-correlation experiment, a continuous-wave spin-lock sequence is employed with a spin-lock field strength of typically 3000–6000 Hz. In order to minimize offset effects, an adiabatic spin-lock pulse can be a useful alternative, as suggested by Mulder *et al.* (*37*) in the rotating frame relaxation measurement. After the buildup of the relaxation interference signal during τ, the S_z magnetization is flipped back to the transverse plane (scheme A), and then the chemical shift labeling of X magnetization takes place during t_1 with simultaneous refocusing of J_{XH} evolution in both experiments. Finally, the antiphase X-coherence which evolves during the subsequent 2δ echo-period is converted to detectable ^{1}H magnetization using the sensitivity enhanced gradient echo–antiecho coherence selection scheme (*33*). Contributions from the undesired coherences are removed by the gradients, e.g., the strong residual antiphase X-magnetization before t_1 is converted with a proton 90° pulse (ϕ_2) to multiple-quantum coherence which is efficiently destroyed by the gradients (G_3, G_4, G_5, and G_6) applied for the desired (X-SQ $\rightarrow$ ^{1}H-SQ) coherence selection. The 16-step phase cycling scheme further enhances the suppression

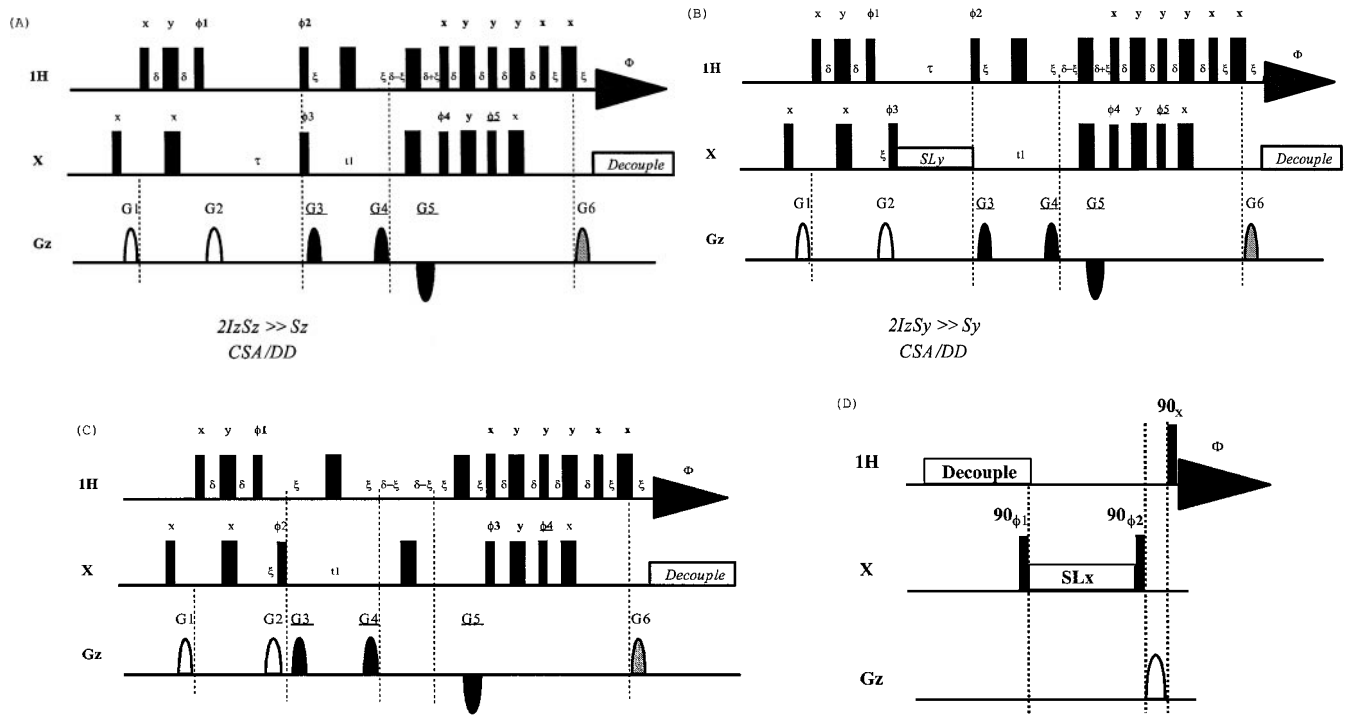

FIG. 1. Summary of the novel, sensitivity enhanced gradient experiments proposed in this study. Thin and thick bars represent 90° and 180° pulses, respectively. Phases are X if not indicated otherwise. The maximum gradient available was ca. 0.5 T/m (100%) and the amplitudes of sine bell-shaped gradients of 1 ms duration with recovery time 200 μs (ξ) are given as a percentage of this value. (A) Longitudinal CSA/DD cross-correlation experiment. (B) Transverse CSA/DD cross-correlation experiment. (C) Reference experiment. The phase cycling was set as $\phi_1 = Y - Y; \phi_2 = X_8 - X_8;\ \phi_3 = -X_4X_4;\ \phi_4 = X_2 - X_2;\ \phi_5 = Y_2 - Y_2$ and $\Phi = X - X_2X - XX_2 - X$; for the reference experiment: $\phi_1 = Y - Y;\ \phi_2 = Y_4 - Y_4;\ \phi_3 = X_2 - X_2;\ \phi_4 = Y_2 - Y_2$ and $\Phi = X - X_2X - XX_2 - X$. Echo–antiecho signals are obtained by alternatively inverting the amplitude of the G_3, G_4, and G_5 gradient pulses and the phase ϕ_5 (ϕ_4 for the reference experiment) of the 90°X pulse for consecutive FIDs. Gradient amplitudes $G_1 = 59$, $G_2 = 49$, $G_3 = 20$, $G_4 = 60$, $G_5 = -80$, $G_6 = 16.22$ for ^{15}N CSA/DD and $G_6 = 40.23$ for ^{13}C CSA/DD experiment. (D) 1D gradient enhanced ortho-ROESY experiment with ^{1}H detection (*35*). $\phi_1 = Y - Y;\ \phi_2 = Y_2 - Y_2$ and $\Phi = X - X_2X$. During the spin-lock pulse (SL_x) of variable duration S_x magnetization is partially converted to $2I_zS_x$ coherence due to CSA/DD relaxation interference. The purging gradient is applied when the interference signal is stored as $2I_zS_z$ coherence. After the last ^{1}H pulse, the antiphase proton magnetization is directly observed.

of unwanted magnetization. Echo–antiecho signals are obtained by performing the experiment twice with the same t_1 and inverting gradients G_3, G_4, and G_5 and the phase ϕ_5 in the second experiment. The reference experiment (Fig. 1C) basically employs the same number of pulses and delay periods as the previous two experiments except that the cross-correlation period τ is omitted. The signal intensity obtained in the reference experiment quantifies the initial INEPT state of the cross-correlation measurement. The cross-correlated relaxation rates (η_{zz} and η_{xy}) are derived by measuring the initial buildup of the interference effect. The relaxation delay τ, in which the cross-correlated relaxation is operative, is typically set to 10, 20, 30, 40, and 50 ms in macromolecules and significantly longer, varying from 10 to 150–200 ms in medium-sized molecules. Contributions from multispin effects due to spatially close ^{1}H dipoles can be neglected, as they do not affect the initial buildup rate of the interference effect.

The pulse schemes of Fig. 1 have been applied to [*2,4,6-*^2H]-α,α-D-trehalose for the measurement of ^{13}C–^{1}H CSA/DD interference at natural abundance of ^{13}C and to a sample of uniformly ^{15}N-enriched human ubiquitin for determining ^{15}N–^{1}H CSA/DD interference. For the present comparative study, the trehalose proved to be an ideal test compound, since its dynamics in a broad temperature range have already been investigated by our group (*38*), and the ^{13}C and ^{1}H CSA projections (geometry dependent CSA_g) are also available from earlier cross-correlation studies (*27*). We found that deuteration in alternating positions is useful to avoid complications arising from interference between ABX type strong coupling and cross-correlation. Representative examples of signal buildup curves as a function of the delay τ obtained by the pulse schemes of Fig. 1 are shown in Fig. 2. For comparison, the transverse cross-correlation rates have been determined by two different methods for each sample; in trehalose the 1D ^{1}H-detected ortho-ROESY (*36*) (Fig. 1D) and in ubiquitin the experiment proposed by Tessari *et al.* (*8*) were also performed. We found that the measured cross-correlation rates showed good agreement within the estimated experimental errors (3–5%), which means that multispin effects are insignificant during the buildup of interference effect. Figures 2a and 2b show the buildup series for C-1 of trehalose. Selected examples

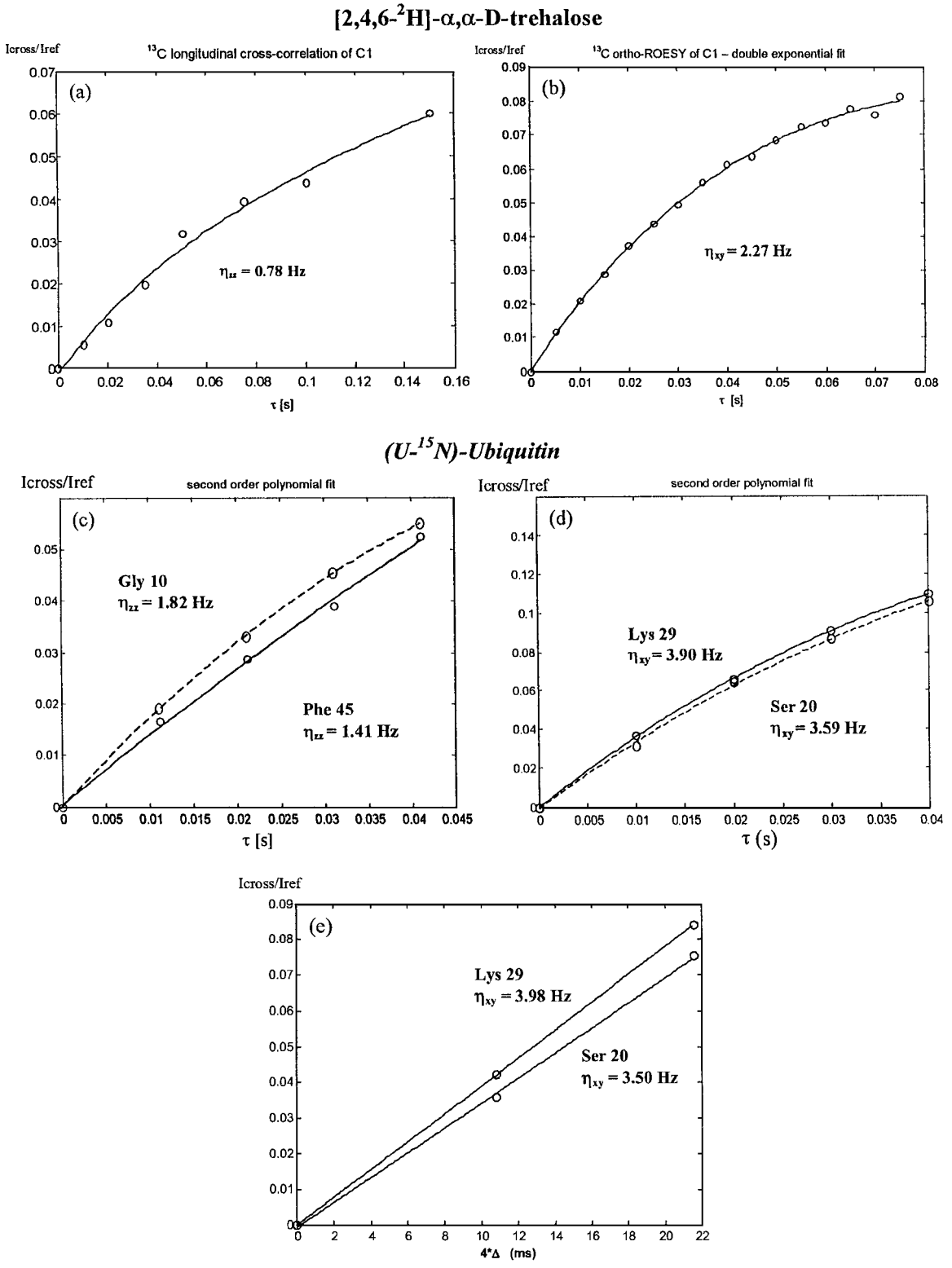

FIG. 2. Buildup of relaxation interference signals in the cross-correlation experiments. The buildup curves (a) and (b) were measured on C1 of [2,4,6-^{2}H]-α,α-D-trehalose using the pulse scheme of Figs. 1A and 1D, respectively. The buildup curves (c), (d), and (e) were obtained on selected residues of [U-^{15}N]-ubiquitin using the pulse sequence of Figs. 1A and 1B and that of Tessari *et al*. (*8*). The experimental conditions are detailed in the text.

of buildup curves for residues of ubiquitin are depicted in Figs. 2c and 2d, together with the signal buildup of the same effects measured by the method of Tessari *et al.* (Fig. 2e). The second-order polynomial fit of the buildup curves was performed using an implementation of the nonlinear least-squares routine in the MATLAB software package (*39*), and the cross-correlation rates (η_{zz} and η_{xy}) were estimated by calculating the first derivative of the best fitted polynomial function at the time origin.

Evaluation of CSA Parameters from the Concerted Use of Five Relaxation Parameters

Besides the longitudinal and transverse cross-correlation rates, the conventional heteronuclear T_1, T_2, and steady-state NOE data were determined in each sample. To this end, the standard 1D *X*-detected relaxation experiments were performed on trehalose and a series of 2D heteronuclear correlated spectra with the gradient sensitivity enhancement scheme of Farrow *et al.* (*40*) was recorded on ubiquitin. Duplicate measurements and/or Monte Carlo analysis have been performed to assess the experimental uncertainty of the relaxation data. The estimated average precision of the experimental data was typically 0.5–1% for T_1, 1–2% for T_2, 2–3% for NOE, and 3–5% for the η_{zz} and η_{xy}. The theoretical expressions for the autorelaxation (R_1, R_2) and cross-correlation rate constants (η_{xy}, η_{zz}) and for the steady-state heteronuclear NOE in terms of the spectral density functions ($J^{\mathrm{a}}(\omega)$, $J^{\mathrm{c}}(\omega)$) are given in Eqs. [1–5] (*26*, *28*).

$$R_1 = 0.1d^2[J^{\mathrm{a}}(\omega_{\mathrm{H}} - \omega_X) + 3J^{\mathrm{a}}(\omega_X) + 6J^{\mathrm{a}}(\omega_{\mathrm{H}} + \omega_X)] + 0.4\,c^2[J^{\mathrm{a}}(\omega_X)] \quad [1]$$

$$R_2 = 0.05d^2[4J^{\mathrm{a}}(0) + J^{\mathrm{a}}(\omega_{\mathrm{H}} - \omega_X) + 3J^{\mathrm{a}}(\omega_X) + 6J^{\mathrm{a}}(\omega_{\mathrm{H}}) + 6J^{\mathrm{a}}(\omega_{\mathrm{H}} + \omega_X)] + (1/15)c^2[3J^{\mathrm{a}}(\omega_X) + 4J^{\mathrm{a}}(0)] \quad [2]$$

$$\mathrm{NOE} = (\gamma_{\mathrm{H}}/\gamma_X)\,0.1d^2[6J^{\mathrm{a}}(\omega_{\mathrm{H}} + \omega_X) - J^{\mathrm{a}}(\omega_{\mathrm{H}} - \omega_X)]/R_1 \quad [3]$$

$$\eta_{xy} = -(\sqrt{3}/15)\,cd[4J^{\mathrm{c}}(0) + 3J^{\mathrm{c}}(\omega_X)] \quad [4]$$

$$\eta_{zz} = -(2\sqrt{3})/5cd\,J^{\mathrm{c}}(\omega_X), \quad [5]$$

where $J^{\mathrm{a}}(\omega) = S^2\tau_{\mathrm{m}}/(1 + \omega^2\tau_{\mathrm{m}}^2) + (1 - S^2)\tau/(1 + \omega^2\tau^2)$ is the autocorrelation spectral density function with the simplifying assumption of isotropic overall tumbling, and $J^{\mathrm{c}}(\omega) = J^{\mathrm{a}}(\omega)(3\cos^2\Theta - 1)/2$ is the cross-correlation spectral density function, where the given relation between the auto- and cross-correlation spectral density function is valid only for small $\Theta(\Theta \leq 30)$. $d = (\mu_0 h\gamma_H\gamma_X)/(8\pi^2 r_{XH}^3$, $c = \gamma_X B_0(\sigma_\parallel - \sigma_\perp)/\sqrt{3}$, in which μ_0 is the vacuum permeability, h is Planck's constant, γ_H and γ_X are the gyromagnetic ratios for ^{1}H and *X*, heteronucleus, respectively, r_{XH} is the internuclear distance, and B_0 is the static magnetic field strength. $\sigma_\parallel$ and $\sigma_\perp$are the principal components (parallel and perpendicular with respect to the CSA axis) of the axially symmetric chemical shielding tensor of *X*, Θ is the angle between the unique axis of the chemical shift tensor and the *X*–H bond vector. $r_{XH} = 0.112$ and 0.102 nm was used for $X = {}^{13}$C and ^{15}N, respectively.

The cross-correlated relaxation (η_{xy}, η_{zz}), as it is evident from Eqs. [4] and [5], depends on the principal values of the chemical shielding tensor, $\Delta\sigma = (\sigma_\parallel - \sigma_\perp)$, the projection angle Θ between the dipole and CSA tensors and also on the dynamics $J(\omega)$ of the molecule. Assuming isotropic tumbling and an axially symmetric chemical shift tensor, we have made attempts to separate contributions due to variations in dynamic and structural factors. Our extension of the Lipari–Szabo approach simply involves a simultaneous fitting of the above five heteronuclear relaxation parameters measured at one field strength in terms of five adjustable variables: the global correlation time τ_{m} and four local parameters, S_i^2, τ_i, $\Delta\sigma_i$, and Θ_i, describing internal motion (S_i^2 and τ_i) and chemical shift anisotropy ($\Delta\sigma_i$ and Θ_i). The experimental relaxation data measured in [2,4,6-^{2}H]-α,α-D-trehalose (1.7 M in D_2O, 275 K), together with the results of the conventional and extended Lipari–Szabo analysis, are given in Table 1. We found that the extended (five parameters, one global and four local) Lipari–Szabo approach did not give a unique, simultaneous solution for the magnitude and orientation of ^{13}C CSA tensors. During several iterations performed with different initial parameters, the individual CSA parameters showed a significant scatter, as demonstrated in Fig. 3. However, the CSA

TABLE 1

The Heteronuclear Relaxation Data Measured in [2,4,6-^{2}H]-α,α-D-Trehalose (1.7 M $D_2$0, T = 275 K) and the Dynamic (S^2, τ_c) and CSA_g Parameters Obtained via the Fitting of Experimental Data Using the Conventional (L–Sz) and the Extended (ext. L–Sz) Lipari–Szabo Approach

	T_1 (s)	T_2 (s)	NOE	η_{zz} (s^{-1})	η_{xy} (s^{-1})	$S^2_{\mathrm{L-Sz}}$	$S^2_{\mathrm{ext.L-Sz}}$	CSA_g (ppm)
C1	0.273 ± .002	0.119 ± .002	0.256 ± .005	0.78 ± .02	2.27 ± .06	0.95	0.90	35.5 ± 2
C3	0.284 ± .002	0.119 ± .002	0.256 ± .005	0.58 ± .02	1.60 ± .05	0.92	0.89	26.4 ± 1
C5	0.285 ± .002	0.117 ± .002	0.236 ± .004	0.86 ± .03	2.30 ± .06	0.93	0.87	38.3 ± 2

Note. The overall correlation time obtained from the conventional and extended Lipari–Szabo analysis using the global fit approach is as follows, $\tau_{\mathrm{c\,L-Sz}} = 1.89$ ns and $\tau_{\mathrm{c\,ext.L-Sz}} = 1.92$ ns, respectively.

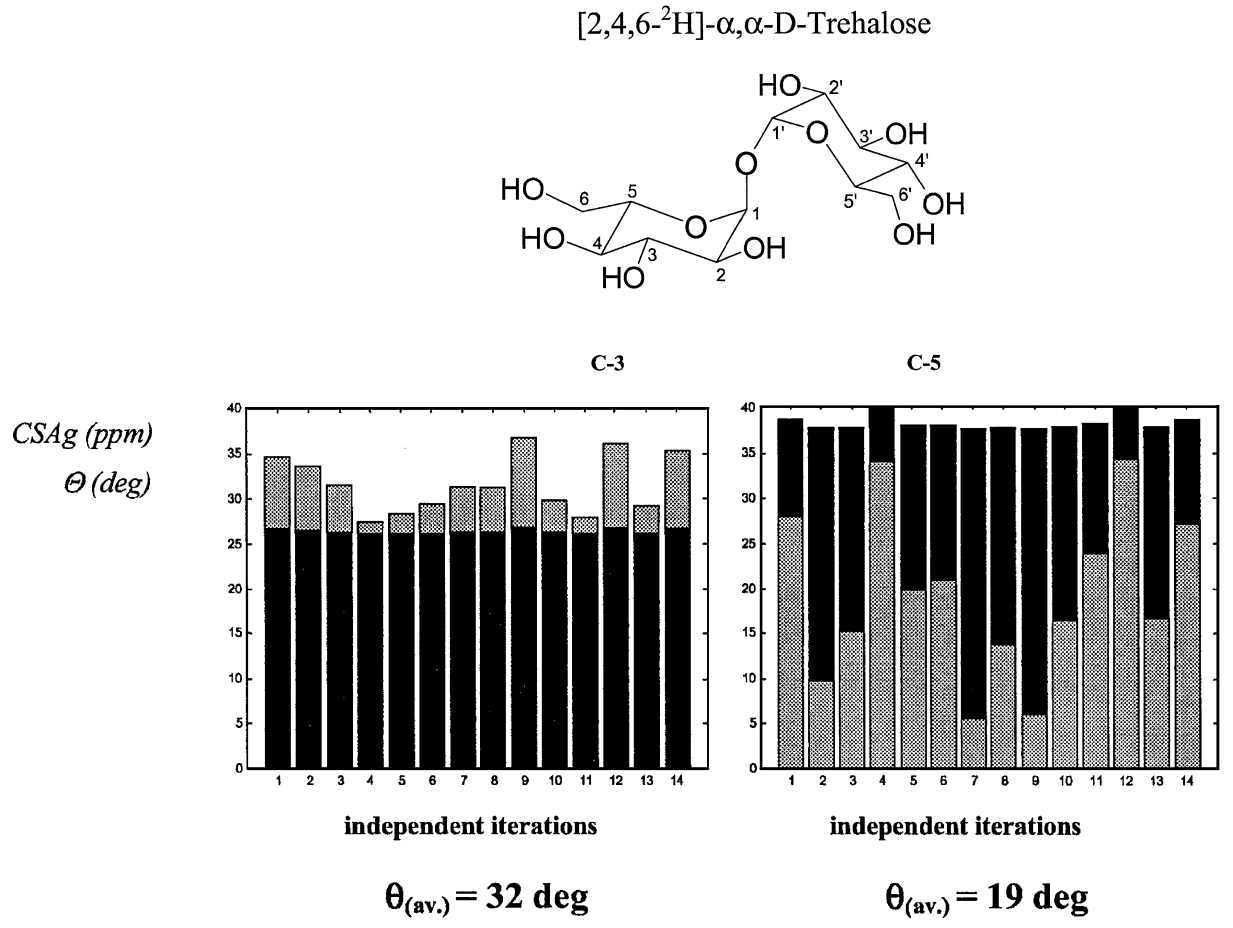

FIG. 3. The result of 14 independent iterative analyses of relaxation data of [2,4,6-^{2}H]-α,α-D-trehalose using the extended Lipari–Szabo approach with randomized initial parameters. The gray bars show the distribution of the CSA angular term (θ) upon successive iterations. The black bars with small variation show the constancy of the geometry dependent CSA_g. The structure of the disaccharide is also shown.

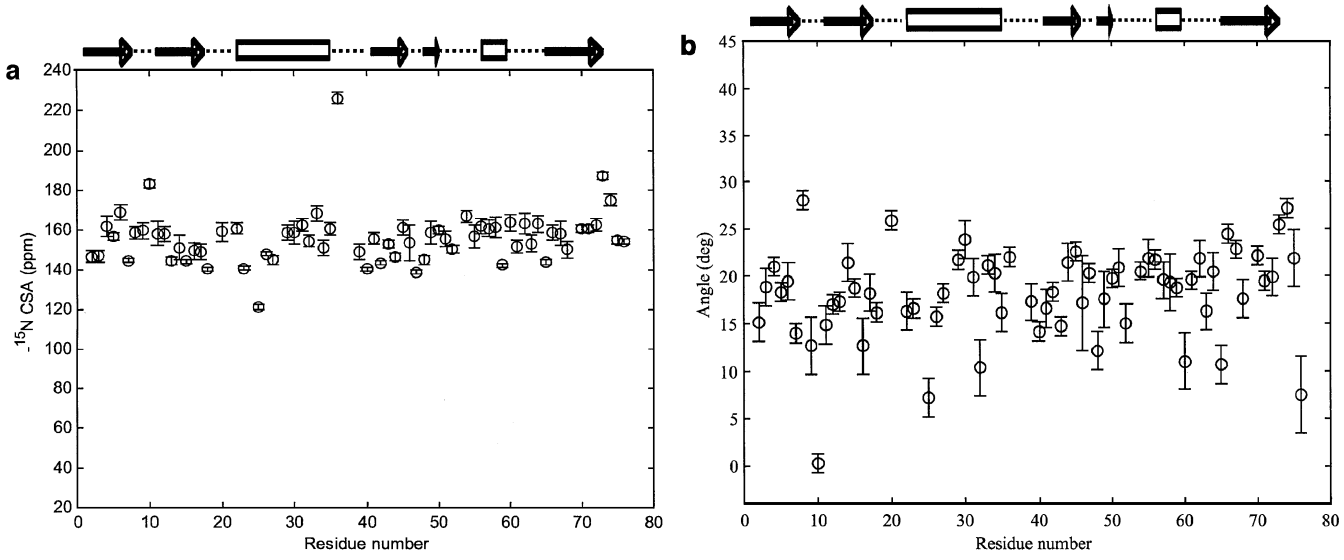

FIG. 4. Sequential distribution of chemical shift anisotropy, ^{15}N CSA (a) and θ (b) in ubiquitin. Error estimates indicated by error bars are obtained from extensive Monte Carlo analysis based on the experimental error of the relaxation data. Secondary structure elements are depicted at the top.

TABLE 2

Selection of Heteronuclear Relaxation Data Measured in [U-^{15}N] Ubiquitin (1.4 mM 95% H_2O : 5% D_2O, T = 300 K) and the Dynamic (S^2, τ_e, τ_c) and ^{15}N CSA (CSA, θ) Parameters Obtained via the Fitting of Experimental Data Using the Extended (ext. L–Sz) Lipari–Szabo Approach

Residue	T_1 (s)	T_2 (s)	NOE	η_{xy} (s^{-1})	η_{zz} (s^{-1})	S^2	τ_e (10^{-12} s)	CSA (ppm)	Θ (deg)
GLN2	*0.476 ± 0.002* (0.99)	*0.171 ± 0.001* (1.04)	*0.67 ± 0.02* (0.97)	*4.07 ± 0.06* (0.99)	*1.48 ± 0.07* (1.01)	0.85	50	−147 ± 3	15 ± 2
ILE3	*0.449 ± 0.003* (0.99)	*0.169 ± 0.003* (1.01)	*0.73 ± 0.02* (0.99)	*4.16 ± 0.11* (0.97)	*1.45 ± 0.03* (1.02)	0.90	29	−147 ± 3	19 ± 2
PHE4	*0.438 ± 0.001* (1.00)	*0.167 ± 0.003* (0.98)	*0.71 ± 0.02* (1.00)	*4.17 ± 0.03* (1.00)	*1.52 ± 0.04* (1.01)	0.88	46	−162 ± 5	21 ± 1
LYS11	*0.514 ± 0.007* (1.01)	*0.204 ± 0.002* (0.99)	*0.52 ± 0.01* (1.01)	*3.71 ± 0.09* (1.00)	*1.37 ± 0.02* (1.01)	0.71	75	−158 ± 6	15 ± 2
ILE23	*0.438 ± 0.005* (0.99)	*0.151 ± 0.005* (1.07)*	*0.74 ± 0.03* (0.99)	*3.96 ± 0.12* (1.06)	*1.58 ± 0.02* (0.99)	0.96	28	−141 ± 1	17 ± 1
ASN25	*0.446 ± 0.001* (0.99)	*0.125 ± 0.002* (1.33)*	*0.70 ± 0.02* (0.96)	*4.22 ± 0.08* (1.00)	*1.54 ± 0.01* (1.01)	0.98	225	−121 ± 1	7 ± 2
LYS33	*0.475 ± 0.005* (1.00)	*0.175 ± 0.004* (1.01)	*0.77 ± 0.04* (1.00)	*3.99 ± 0.04* (1.00)	*1.39 ± 0.03* (1.04)	0.81	0	−168 ± 4	21 ± 1
ILE36	*0.527 ± 0.006* (0.97)	*0.185 ± 0.003* (1.04)	*0.80 ± 0.03* (0.97)	*4.00 ± 0.02* (1.00)	*1.40 ± 0.07* (1.04)	0.62	0	−226 ± 3	22 ± 1
ARG54	*0.485 ± 0.002* (0.99)	*0.169 ± 0.002* (1.05)	*0.77 ± 0.03* (0.99)	*4.32 ± 0.10* (0.92)	*1.39 ± 0.02* (1.03)	0.80	0	−167 ± 3	21 ± 1

Note. The numbers *in italics* are the measured experimental relaxation data. The bracketed numbers denote the ratio of the calculated and experimental relaxation data. The overall correlation time obtained from the extended Lipari–Szabo analysis using the global fit approach is $\tau_c = 4.0$ ns.

* Residues involved in conformational exchange.

projections ($CSA_g = \Delta\sigma(3\cos^2\Theta - 1)/2$) remained stable during the iterations regardless of the applied initial parameters of the least-squares minimization. The ^{13}C CSA_g values obtained are in good agreement with our earlier data. The global correlation time has become longer and the individual order parameters (S_i^2) have slightly decreased in comparison with the conventional Lipari–Szabo analysis. However, due to the small magnitude of ^{13}C CSA and the limited number of measurable parameters in trehalose, our attempts to separate the CSA magnitude and angular terms have failed. Potentially, the CSA_g could be also a useful parameter, since quantum-chemical calculations of the shielding tensor require careful geometry optimization, hence inherently provide the experimentally available CSA_g parameter. In principle, it is possible to derive the individual values of ^{13}C CSA parameters if additional relaxation data are measured at higher fields where the CSA contribution to ^{13}C relaxation becomes enhanced. To the best of our knowledge, this study presents the first attempt for simultaneous evaluation of the dynamics and CSA parameters in carbohydrates.

In contrast, the extended Lipari–Szabo analysis of ^{15}N relaxation data measured for ^{15}N-labeled ubiquitin (1.4 mM, pH 4.7, 95% : 5% = $H_20 : D_2O$, 600 MHz ^{1}H frequency, 300 K) led to a unique solution for both the dynamic and the CSA parameters. As a result of the global fit approach (*41*) of the five relaxation parameters, we found that the ^{15}N CSA varies between −121 and −226 ppm with an average of −156 ppm, and the angle Θ shows a distribution between 0 and 28° with an average of 18°. These values, in agreement with the findings of Fushman *et al.* (*19*), indicate that the ^{15}N CSA is not constant along the residues of a protein, exhibiting a substantial variation, as demonstrated in Fig. 4. Selected examples of the measured relaxation data and the calculated dynamic and CSA parameters are given in Table 2. Comparing the ^{15}N CSA values obtained from the extended Lipari–Szabo analysis with those of Fushman *et al.* (*19*), we found that for 75–80% of the residues the agreement is fairly good, and the CSA values agree within ±10–13 ppm. In the case of eight residues, however, a larger difference (>30 ppm) is found between the data of appropriate residues. The explanation for these substantial differences is still unknown. The high sensitivity of the multiple-field approach to experimental errors in the η_{xy}/R_2 ratios would be one possible explanation (*42*). The order parameters obtained from the extended Lipari–Szabo analysis agree within ±2–3% with those of the conventional approach. Note that significantly larger differences can be expected for bigger molecules at higher magnetic fields (*45*) due to the quadratic field dependence of CSA relaxation. A complete set of the measured ^{15}N relaxation data together with the derived dynamic and ^{15}N CSA parameters is given in the *supplementary material*[2].

Recently, a different approach based on the measurement of ^{15}N chemical shift changes between an isotropic and a liquid crystalline phase (*46*, *47*) has been used for the determination of the average values of the magnitude and orientation of ^{15}N chemical shielding tensors. The residue-specific values for ^{15}N CSA

[2] Two tables containing T_1, T_2, NOE, and cross-correlation rates of ubiquitin at 300 K from 600-MHz spectra (Table 3) and the calculated dynamic and ^{15}N CSA parameters (Table 4) are available from the authors.

can only be obtained if the chemical shift changes are measured for at least two different orientations of the alignment tensor and if the orientation of the CSA tensor is assumed to be constant, as well as if an accurate NMR structure of the molecule is available. Since the experimental requirements differ for the aligned phase and the cross-correlation methods, they may be considered complementary approaches. The former yields average CSA values (which may depend on secondary structure) and attempts to derive residue specific CSAs by that approach failed (*46*). The average ^{15}N CSAs for the two approaches are -163 ± 4 ppm (64 residues) (*46*) and -156 ± 13 ppm (67 residues, this work).

CONCLUSIONS

New, sensitivity enhanced gradient methods have been used for the measurement of the longitudinal and transverse cross-correlation rate constants. The pulse schemes are applicable to molecules of any size and do not necessarily require specific isotopic enrichment. In these experiments complications arising from multispin effects are avoided by the use of the initial rate approach. We have found that the ortho-ROESY and other transverse cross-correlation experiments provide the same rate constants in ubiquitin within the estimated experimental error. However, in the case of trehalose, the conventional transverse experiment (*8*) has failed in our hands.

We have shown that an extension of the Lipari–Szabo model-free formalism which is based on the concerted use of five heteronuclear relaxation parameters (T_1, T_2, NOE, η_{zz}, and η_{xy}) measured at one magnetic field strength can be successfully used to simultaneously evaluate the dynamics and ^{15}N CSA parameters in ubiquitin. A separation of the magnitude and orientation of the chemical shift tensor could be achieved, assuming axial symmetry for CSA tensors and isotropic tumbling of the molecule. We found that ^{15}N CSA is not uniform in ubiquitin. The agreement with Fushman *et al. (19)* is generally good with a few exceptions.

EXPERIMENTAL

All NMR experiments were carried out on Bruker Avance DRX 500 and 600 spectrometers operating at 500 and 600 MHz ^{1}H frequency, respectively, equipped with a pulsed field gradient ^{1}H/^{13}C/^{15}N triple-resonance probe. The 1D INEPT-enhanced ^{13}C-detected T_1, T_2 (*43*), and steady-state {^{1}H}–^{13}C NOE measurements were performed on 1.7 M [2,4,6-^{2}H]-α,α-D-trehalose in D_2O at 500 MHz and 275 K using the following experimental parameters: relaxation delay times for T_1: 0.001, 0.01, 0.02, 0.04, 0.06, 0.08, 0.12, 0.16, 0.2, 0.26, 0.32, 0.48, 0.64, 0.96, 1.28, and 2.56 s, number of transients 128, recycle delay 3 s; relaxation delay times for T_2: 1, 1.7, 3.4, 6.8, 13.7, 27.4, 54.8, 109.6, 219.1, and 438.3 ms, number of transients 128, recycle delay 3 s; NOE on/off spectra were recorded in an interleaved manner with 1024 transients, using a recycle delay of 3 s and applying the Waltz-16 decoupling scheme for ^{1}H saturation in the NOE on experiment. T_1 and T_2 were extracted using the three- and two-parameter monoexponential fits of the measured peak intensities. The statistical error of the relaxation data was estimated from duplicate experiments or randomized data using Monte Carlo simulations. The ^{13}C CSA/DD cross-correlation measurements were performed with ^{1}H detection using the following experimental parameters: 1D ortho-ROESY (Fig. 1D) for C1, C3, and C5 on-resonance with 0.1, 5, 10, 15, 20, 25, 30, 35, 40, 45, 50, 55, 60, 65, 70, and 75 ms duration of SL pulse (4166 Hz) and 256 number of transients per experiment allowing a recycle delay of 4 s. 2D experiments were acquired with relaxation delay times 10, 20, 30, 40, and 50 ms, spectral widths 751 and 629 Hz in F_2 and F_1, respectively, and 64 transients per t_1 increment with a recycle delay of 2.5 s. A spin-lock field of 5952 Hz was used for the 2D ^{13}C transverse cross-correlated relaxation measurement. The 2D longitudinal cross-correlation experiment was performed with relaxation delay times of 10, 20, 35, 50, 75, 100, and 150 ms. A cosine-squared window function and zero-filling were applied in both dimensions prior to 2D Fourier transformation. A second-order polynomial fitting was applied to the time course of the measured peak intensities in order to extract the cross-correlation rate constants using the initial rate approach.

The ^{15}N relaxation data (60 MHz) of 1.7 mM ^{15}N-labeled ubiquitin (95% : 5% = H_2O : D_2O, pH 4.7, purchased from VLI Research, Southeastern, PA) at 300 K were measured with a series of 2D heteronuclear correlated spectra using the sensitivity enhanced gradient pulse schemes of Farrow *et al*. (*40*), Tessari *et al*. (*8*), and Fig. 1. The resonance assignments were taken from Wang *et al*. (*44*). The spectral widths were 7180 and 1560 Hz in F_2 and F_1, respectively. The ^{1}H carrier frequency was placed at the water resonance and at 116.6 ppm for ^{15}N. The relaxation delay times were as follows for T_1: 11.2, 101.2, 201.2, 401.2, 601.2, 801.2 ms; for T_2, CPMG pulse trains of 0.03, 16.5, 49.6, 99.3, 148.9, and 198.5 ms in length were used; for η_{zz} and η_{xy}, the cross-correlation was active for 11.2, 21.2, 31.2, and 41.2 ms. The number of transients collected per t_1 increment was 16 for T_1 and T_2, 32 for NOE, and 64 for η_{zz} and η_{xy} measurements. A spin-lock field of 3400 Hz was used for the ^{15}N transverse cross-correlation experiment. Two-parameter exponential fits of the measured peak intensities were applied to extract the relaxation time constants T_1 and T_2. The cross-correlation rate constants were determined using the initial rate approach. Monte Carlo error analysis (300–500 steps) was performed to assess the effect of the estimated errors of the experimental data on the fitted parameters of the extended Lipari–Szabo analysis.

ACKNOWLEDGMENTS

K.E.K. and Gy.B. thank the National Research Foundation for financial support (OTKA T 029089 to K.E.K. and Gy.B. and OTKA T 034515 to K.E.K.). OMFB Mec-93-0098, Phare-Accord H-9112-0198, and OTKA A084 supported the purchase of the DRX 500 spectrometer used in the study. For the use of DRX 600, we thank Victor J. Hruby and Neil Jacobsen (Tucson, AZ).

Support for methodological development provided by FKFP 500/1997, by EC Grant IC15CT96-0903 (Inco-Copernicus), and by the International Center for Genetic Engineering and Biotechnology CRP/HUN97-01(t2) is gratefully acknowledged.

REFERENCES

1. V. A. Daragan and K. H. Mayo, Tri- and diglycine backbone rotational dynamics investigated by ^{13}C NMR. multiplet relaxation and molecular dynamics simulations, *Biochemistry* **32,** 11488–11499 (1993).
2. L. G. Werbelow, "Encyclopedia of Nuclear Magnetic Resonance" (D. M. Grant and R. K. Harris, Eds.), Vol. 6, pp. 4072–4078, Wiley, London, 1996.
3. A. G. Palmer, Probing molecular-motion by NMR, *Curr. Opin. Struct. Biol.* **7,** 732–737 (1997).
4. N. Tjandra and A. Bax, Large variations in $^{13}C_\alpha$ chemical shift anisotropy in proteins correlate with secondary structure, *J. Am. Chem. Soc*. **119,** 9576–9577 (1997).
5. N. Tjandra and A. Bax, Solution NMR measurement of amide proton chemical shift anisotropy in ^{15}N-enriched proteins. Correlation with hydrogen bond length, *J. Am. Chem. Soc*. **119,** 8076–8082 (1997).
6. B. Reif and M. Hennig, Direct measurement of angles betwen bond vectors in high-resolution NMR, *Science* **276,** 1230–1233 (1997).
7. M. Tessari, H. Vis, R. Boelens, R. Kaptein, and G. W. Vuister, Quantitative measurement of relaxation interference effects between $^1H(N)$ CSA and ^1H–^{15}N dipolar interaction: Correlation with secondary structure, *J. Am. Chem. Soc*. **119,** 8985–8990 (1997).
8. M. Tessari, F. A. A. Mulder, R. Boelens, and G. W. Vuister, Determination of amide proton CSA in ^{15}N-labeled proteins using ^1H CSA/^{15}N–^1H dipolar and ^{15}N CSA/^{15}N–^1H dipolar cross-correlation rates, *J. Magn. Reson*. **127,** 128–133 (1997).
9. D. W. Yang and L. E. Kay, Determination of the protein backbone dihedral angle ψ from a combination of NMR-derived cross-correlation spin relaxation rates, *J. Am. Chem. Soc*. **120,** 9880–9887 (1998).
10. R. Ghose, K. Huang, and J. H. Prestegard, Measurement of cross correlation between dipolar coupling and chemical shift anisotropy in the spin relaxation of ^{13}C, ^{15}N-labeled proteins, *J. Magn. Reson*. **135,** 487–499 (1998).
11. C. Kojima, A. Ono, M. Kainosho, and T. L. James, Quantitative measurement of transverse and longitudinal cross-correlation between ^{13}C–^1H dipolar interaction and ^{13}C chemical shift anisotropy: Application to a ^{13}C-labeled DNA duplex, *J. Magn. Reson*. **136,** 169–175 (1999).
12. M. J. J. Blommers, W. Stark, C. E. Jones, D. Head, C. E. Owen, and W. Jahnke, Transferred cross-correlated relaxation complements transferred NOE: Structure of an IL-4R-derived peptide bound to STAT-6, *J. Am. Chem. Soc*. **121,** 1949–1953 (1999).
13. I. C. Felli, C. Richter, C. Griesinger, and H. Schwalbe, Determination of RNA sugar pucker mode from cross-correlated relaxation in solution NMR spectroscopy, *J. Am. Chem. Soc*. **121,** 1956–1957 (1999).
14. G. Lipari and A. Szabo, Model-free approach to the interpretation of nuclear magnetic resonance relaxation in macromolecules. 1. Theory and range of validity 2. Analysis of experimental results, *J. Am. Chem. Soc*. **104,** 4546–4559 (1982).
15. G. Lipari and A. Szabo, Model-free approach to the interpretation of nuclear magnetic-resonance relaxation in macromolecules. 2. Analysis of experimental results, *J. Am. Chem. Soc*. **104,** 4559–4570 (1982).
16. D. M. Lemaster, Larmor frequency-selective model-free analysis of protein NMR relaxation, *J. Biomol. NMR* **6,** 366–374 (1995).
17. G. M. Clore, A. Szabo, A. Bax, L. E. Kay, P. C. Driscoll, and A. M. Gronenborn, Deviations from the simple two-parameter model-free approach to the interpretation of nitrogen-15 nuclear magnetic relaxation of proteins, *J. Am. Chem. Soc*. **112,** 4989–4991 (1990).
18. D. Fushman and D. Cowburn, Model-independent analysis of ^{15}N chemical shift anisotropy from NMR relaxation data. Ubiquitin as a test example, *J. Am. Chem. Soc*. **120,** 7109–7110 (1998).
19. D. Fushman, N. Tjandra, and D. Cowburn, Direct measurement of ^{15}N chemical shift anisotropy in solution, *J. Am. Chem. Soc*. **120,** 10947–10952 (1998).
20. A. L. Lee and A. J. Wand, Assessing potential bias in the determination of rotational correlation times of proteins by NMR relaxation, *J. Biomol. NMR* **13,** 101–112 (1999).
21. C. Scheurer, N. R. Skrynnikov, S. F. Lienin, S. K. Straus, R. Brüschweiler, and R. R. Ernst, Effects of dynamics and environment on ^{15}N chemical shielding anisotropy in proteins. A combination of density functional theory, molecular dynamics simulation, and NMR relaxation, *J. Am. Chem. Soc*. **121,** 4242–4251 (1999).
22. C. D. Kroenke, J. P. Loria, L. K. Lee, M. Rance, and A. G. Palmer, Longitudinal and transverse ^1H–^{15}N dipolar ^{15}N chemical shift anisotropy relaxation interference: Unambiguous determination of rotational diffusion tensors and chemical exchange effects in biological macromolecules, *J. Am. Chem. Soc*. **120,** 7905–7915 (1998).
23. G. Barbato, M. Ikura, L. E. Kay, R. W. Pastor, and A. Bax, Backbone dynamics of calmodulin studied by ^{15}N relaxation using inverse detected two-dimensional NMR spectroscopy: The central helix is flexible, *Biochemistry* **31,** 5269–5278 (1992).
24. R. Brüschweiler, X. B. Liao, and P. E. Wright, Long-range motional restrictions in a multidomain zinc-finger protein from anisotropic tumbling, *Science* **268,** 886–889 (1995).
25. N. Tjandra, S. E. Feller, R. W. Pastor, and A. Bax, Rotational diffusion anisotropy of human ubiquitin from ^{15}N NMR relaxation, *J. Am. Chem. Soc*. **117,** 12562–12566 (1995).
26. M. Goldman, Interference effects in the relaxation of a pair of unlike spin-1/2 nuclei, *J. Magn. Reson*. **60,** 437–452 (1984).
27. G. Batta, K. E. Kövér, and J. Kowalewski, A comparison of 1D and 2D (unbiased) experimental methods for measuring CSA/DD cross-correlated relaxation, *J. Magn. Reson*. **136,** 37–46 (1999).
28. A. Abragam, "Principles of Nuclear Magnetism," Oxford Univ. Press, Oxford, U.K., 1961.
29. N. Tjandra, A. Szabo, and A. Bax, Protein backbone dynamics and ^{15}N chemical shift anisotropy from quantitative measurement of relaxation interference effects, *J. Am. Chem. Soc*. **118,** 6986–6991 (1996).
30. R. Ghose and J. H. Prestegard, Improved estimation of CSA-dipolar coupling cross-correlation rates from laboratory frame relaxation experiments, *J. Magn. Reson*. **134,** 308–314 (1998).
31. G. Jaccard, S. Wimperis, and G. Bodenhausen, Observation of $2I_zS_z$ order in NMR relaxation studies for measuring cross-correlation of chemical-shift anisotropy and dipolar interactions, *Chem. Phys. Lett*. **138,** 601–606 (1987).
32. Z. W. Zheng, C. L. Mayne, and D. M. Grant, Ethanol molecular-dynamics measured by coupled spin relaxation exhibiting cross-correlation between dipole–dipole and chemical-shift anisotropy, *J. Magn. Reson. A* **103,** 268–281 (1993).
33. L. E. Kay, P. Keifer, and T. Saarinen, Pure absorption gradient enhanced heteronuclear single quantum correlation spectroscopy with improved sensitivity, *J. Am. Chem. Soc*. **114,** 10663–10665 (1992).
34. G. Batta and J. Gervay, Solution-phase ^{13}C and ^1H chemical-shift anisotropy of sialic-acid and its homopolymer (colominic acid) from cross-correlated relaxation, *J. Am. Chem. Soc*. **117,** 368–374 (1995).
35. G. Batta, K. E. Kövér, and J. Kowalewski, *in* "NATO Advanced Research Workshop Series, Applications of NMR to the Study of the Structure and Dynamics of Supramolecular Complexes," Sitges, Spain, 5–9 May, 1998 (M. Pons, Ed. NMR in Supramolecular Chemistry), Kluwer, Dordrecht, 1998.

36. R. Brüschweiler and R. R. Ernst, Molecular-dynamics monitored by cross-correlated cross relaxation of spins quantized along orthogonal axes, *J. Chem. Phys*. **96,** 1758–1766 (1992).

37. F. A. A. Mulder, R. A. de Graaf, R. Kaptein, and R. Boelens, An off-resonance rotating frame relaxation experiment for the investigation of macromolecular dynamics using adiabatic rotations, *J. Magn. Reson*. **131,** 351–357 (1998).

38. G. Batta, K. E. Kövér, J. Gervay, M. Hornyák, and G. M. Roberts, Temperature dependence of molecular conformation dynamics, and chemical shift anisotropy of α,α-trehalose in D_2O by NMR relaxation, *J. Am. Chem. Soc*. **119,** 1336–1345 (1997).

39. "MATLAB Reference Guide," Math Works, Natick, MA, 1997.

40. N. A. Farrow, R. Muhandiram, A. U. Singer, S. M. Pascal, C. M. Kay, G. Gish, S. E. Shoelson, T. Pawson, J. D. Forman-Kay, and L. E. Kay, Backbone dynamics of a free and a phosphopeptide-complexed Src homology 2 domain studied by ^{15}N NMR relaxation, *Biochemistry* **33,** 5984–6003 (1994).

41. M. J. Dellwo and A. J. Wand, Model-independent and model-dependent analysis of the global and internal dynamics of cyclosporine-A, *J. Am. Chem. Soc*. **111,** 4571–4578 (1989).

42. C. Renner and T. A. Holak, Separation of anisotropy and exchange broadening using ^{15}N CSA-^{15}N–^{1}H dipole–dipole relaxation cross-correlation experiments, *J. Magn. Reson*. **145,** 192–200 (2000).

43. K. E. Kövér, P. Forgó, and G. Batta, Rapid method for combined X–{^{1}H} NOE and T_1 measurement using heteronuclear polarization transfer, *Magn. Reson. Chem*. **33,** 871–873 (1995).

44. A. C. Wang, S. Grzesiek, R. Tschudin, P. J. Lodi, and A. Bax, Sequential backbone assignment of isotopically enriched proteins in D_2O by deuterium-decoupled HA(CA)N and (CACO)N, *J. Biomol. NMR* **5,** 376–382 (1995).

45. J. Czernek, R. Fiala, and V. Sklenar, Hydrogen bonding effects on the ^{15}N and ^{1}H shielding tensors in nucleic acid base pairs, *J. Magn. Reson*. **145,** 142–146 (2000).

46. G. Cornilescu and A. Bax, Measurement of proton, nitrogen, and carbonyl chemical shielding anisotropies in a protein dissolved in a dilute liquid crystalline phase, *J. Am. Chem. Soc*. **122,** 10143–10154 (2000).

47. J. Boyd and C. Redfield, Characterization of N-15 chemical shift anisotropy from orientation-dependent changes to N-15 chemical shifts in dilute bicelle solutions, *J. Am. Chem. Soc*. **121,** 7441–7442 (1999).